JGR Space Physics

TECHNICAL REPORTS: METHODS

10.1029/2020JA028418

The Application of a Deep Convolutional Generative Adversarial Network on Completing Global TEC Maps

Jie Chen[1], **Hanxian Fang**[1], **and Zhendi Liu**[1]

[1]College of Meteorology and Oceanography, National University of Defense Technology, Nanjing, China

Key Points:

- This study adopts an improved Generative Adversarial Network with a local discriminator and a global discriminator to completing the TEC maps with missing data
- The completion network of Global and Local GAN is able to complete arbitrary regions on the images
- The model achieves better performance in the more complicated structures during geomagnetic storm time

Correspondence to:

H. Fang,
fanghx@hit.edu.cn

Citation:

Chen, J., Fang, H., & Liu, Z. (2021). The application of a deep convolutional generative adversarial network on completing global TEC maps. *Journal of Geophysical Research: Space Physics*, *126*, e2020JA028418. https://doi.org/10.1029/2020JA028418

Received 9 JUL 2020
Accepted 30 OCT 2020

Abstract Total electron content (TEC) map is one of the important ionospheric parameters. The International Global Navigation Satellite System Service (Ionosphere Working Group) provides the combined vertical TEC maps. However, the postprocessing of the IGS TEC maps may cost quite a long time, and it's not easy for the organization to collect the complete data. It is necessary for researchers to figure out a method to complete the global TEC maps efficiently with regard to the problems of lack of data or not available to the standard IGS TEC. With the rapid development of the deep learning methods, the Deep Convolutional Generative Adversarial Network exhibits the great potential in computer vision. In this paper, we propose a new method called Global and Local GAN (GLGAN) based on the DCGAN and apply it on completing the global TEC maps. Different from the traditional GAN, the GLGAN consists of a generator (or called completion network) and two discriminators. The completion network is powerful enough to Extract features of IGS TEC maps to complete the TEC maps. The design of two discriminators enhances the ability of judging the quality of output images, and improves the accuracy of the completion network. After analyzing the results, we find the GLGAN have a better performance in complicate structures during geomagnetic storm time. The success of the GLGAN in completing the TEC maps suggests that the deep learning methods are able to solve many problems regarding to data and images in ionospheric parameters' reconstruction or forecasting.

1. Introduction

Total electron content (TEC) representing the integrated electron density from satellites to the receivers is one of the important parameters which can monitor the condition of space weather and provide valuable information for navigation improvement (Coster et al., 2008). With the rapid development of the technologies of ionospheric observation, such as the GPS-based measurement (Jakowski et al., 2002) and ground-based measurement, a mass of TEC data are available. Benefit from the continuous observation of GPS receivers, researchers produce global maps of total electron content (TEC-map) at hours interval (Mannucci et al., 1998). To generate the reliable TEC global maps, the International GNSS Service Ionosphere Working Group is set up in 1998 (Feltens, 2003). After the raw data are measured by the GNSS ground network, several independent computation centers compute the distribution of TEC worldwide, and the analysis centers will evaluate these TEC maps. Finally, the Ionospheric Associate Combination Center combines the products above and generate the reliable VTEC map, Vertical Total Electron Content map (Hernández-Pajares et al., 2009). Since 1998, IGS has provided abundant continuous global VTEC maps for space physics research.

However, challenges still occur due to the lack of ground receivers, especially over the oceans and Southern Hemisphere (Rao et al., 2019). It is hard for other institutes or communities except IGS to fill data in these areas exactly concerning the complexity of the process to generate the IGS TEC. Fortunately, the flourish of Deep Learning during these years may bring a breakthrough to this problem. Despite the traditional interpolation methods (Orús et al., 2005), the Generative Adversarial Networks (GAN) in Deep Learning may provide a new way to solve the problem of data lack. Owing to the improvement of convolutional neural networks (Chua et al., 1993; Krizhevsky et al., 2012) and the progress of optimization algorithms, the generative models such as GAN (Goodfellow et al., 2014) can characterize the structure of the pictures and figure out the possibility distribution of input data. Learning from the training set, GAN is able to train a discriminator and a generator to map a probability distribution which approaches the real picture's (Radford et al., 2015). Thus, GANs can generate the artificial samples almost same as those in the training set. Based

on the GAN, a mess of improved GANs have shown their special capabilities with regard to the special tasks. For example, the conditional GAN (CGAN) can solve the conditional probability problems (E.un-Young Ji et al., 2020) regardless of the complex structure which has been applied to reconstruct the cloud vertical profile (Leinonen et al., 2019). What's more, deep convolutional generative adversarial networks (DCGAN) is developed based on the success GANs, which combines the CNNs and GANs (Ledig et al., 2016). In space physics, a regularized deep convolutional generative adversarial network (RDCGAN) is proposed to manipulate the image completion of the TEC maps (Chen et al., 2019). However, the RDCGAN generates the brand-new picture, which means not only the data-lacking area but also the original parts filled with raw data are covered by the generated picture. And the RDCGAN can only train the model aiming at certain areas, which requires the pre-completed images are aligned to the learning patches (Deng et al., 2011). In addition, the traditional GANs generate the new picture simply from a probability distribution such as Gaussian probability distribution, which will lead to the instability during learning (Salimans et al., 2016).

With regard to the image completion task, a highly performed network model has been proposed which can solve or alleviate the problems above. Based on the GAN as well, Globally and Locally Consistent Image Completion method (GLCIC) has achieved success in completing human face images and scenery images (Iizuka et al., 2017). GLCIC consists of a completion network, a local discriminator and a global discriminator. This kind of GAN proved to be critical in receive locally coherent images. Additionally, instead of training pure generative models, we tuning the training process to make the stability a priority. In this paper, we propose the application of Global and Local GAN (GL-GAN) on global TEC map completion. The advantages of this approach are obvious when it is applied to the space physics. As is known to all, the area of equatorial anomaly on the TEC map varies strongly depending on different space environment. And the structure of such areas are very complex. If we only adopt the traditional methods, it would be hard to restore the complicated structure. However, Global and Local GAN (GLGAN) has shown better performance on completing pictures with complicated structures, such as generating the human face images.

2. Architecture of Global and Local GAN

This method is based on the deep convolutional neural networks to fulfill the completion task of global TEC maps. According to the GAN principle, this kind of neural network consists of a generator and a discriminator. Considering the matching of the local completion area and the global map, our approach adopts two discriminators. While the generator is trained to fool the discriminators, the discriminators are trained to distinguish whether the generated map is real or fake.

2.1. Convolutional Neural Network

Convolutional neural network (Fukushima et al., 1998) is a deep feed forward neural network characterized by local connection and weight sharing. At present, the convolutional neural network is generally a feed forward neural network formed by stacking convolutional layers, pooling layers and fully connected layers, which is trained by the back propagation algorithm. A cluster of filters are convoluted with the input map to generate the output map. With several convolution process, the final output is always expressed as a non-linear activation function, such as the Rectified Linear Unit (ReLU). We also adopt a variation of the standard convolution layers which are called the dilated convolution layers (Yu and Koltun, 2015). The dilated convolution is a method to increase output unit receptive field without increasing the number of parameters. Finally, the loss function of the corresponding input data set and output maps obtained from the network are minimized with the back-propagation algorithm. The loss function is used to describe the distance between the training model's output and the real maps in data set. When the decrease of loss function of each step is smaller than a threshold value, we think the network has been well trained and the training process will be interrupted.

2.2. Completion Network

In this study, the generator of this GAN is also known as the completion network, which is aimed at the local completion of the TEC maps. The completion network is based on the convolutional network. An overview of the network architecture is clearly displaced in Figure 1. Generally, the traditional generator of

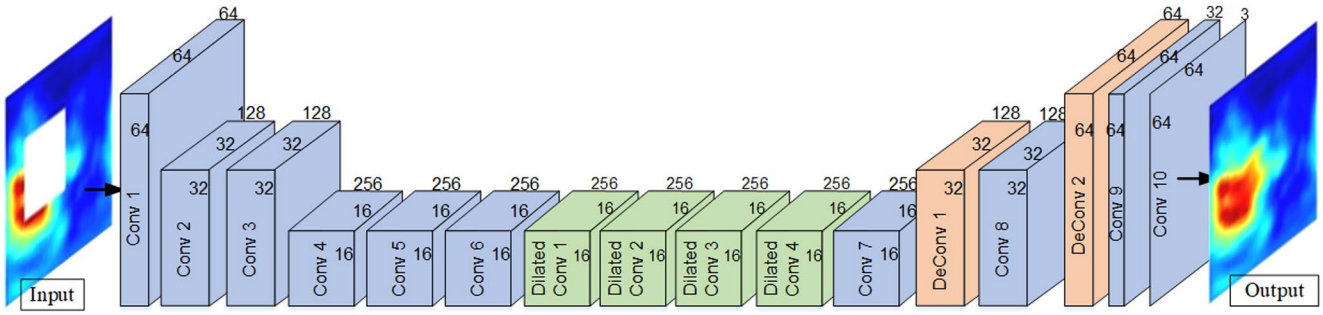

Figure 1. Overview of the completion network of the GLGAN. The completion network contains three kinds of convolutional layers: the normal convolutional layer, the dilated convolutional layer, the deconvolutional layer. The input of the impletion network is the masked image and the output is the completed image with the same length and width. GLGAN, Global and Local GAN.

GANs only has a decoder structure which contains several deconvolution layers to generate the map from a certain probability distribution. This kind of GANs generate brand new map, which are failed to reserve the information of the original maps and thus are unable to satisfy the task of local completion. The generator of our GAN contains both the coder and decoder structures, which means the input is an incomplete map and the output is a complete map. As a result, the original information of the part without being completed can be restored in the output map.

Instead of using many pooling layers, our completion network adopts several stride convolutional layers. The application of the stride convolution layers is an important method to avoid the blurry texture of the completion part. Compared with the pooling layers the stride convolution layers perform better in obtaining detailed structures of the map. Dilated convolutional layers are also adopted in the completion network. Dilated convolution is also known as convolution with holes. By adding holes on the standard convolution map, the network will achieve a larger reception field, and a new hyper-parameter named dilation rate is used to describe the number of intervals in the kernel. By means of dilated convolution, each output pixel will be computed without adding extra parameters.

2.3. Discriminator

The discriminator of GAN is an important network to discriminate whether the generated map is real or fake. Considering the task of discriminator, the ability of discriminator should be little stronger than the generator. During each iteration, the discriminator and the generator will be updated at the same time. In this method, we adopt a global discriminator and a local discriminator to control the quality of the generated maps. Both of the discriminators are based on the standard convolutional neural networks that turn the image into a vector. An overview of the discriminators is displaced in Figure 2.

The total image which is rescaled to 64×64 pixels is taken as input of the global discriminator. After six convolution layers and a fully connected layer, the image is converted to a 1024-dimension vector. All of the convolution layers adopt the stride convolution, and the stride is equal to 2×2 pixel. The local discriminator has a familiar structure with the global discriminator, which is also based on the convolution layers. However, the input of the local discriminator is an image of 32×32 pixel. The input image is a patch selected around the completed area. After five convolution layers and a fully connected layer, the image is also converted to a 1024-dimension vector.

The advantage of adopting two local and global discriminators is obvious. Different from the traditional GANs that generate the whole new map, our task is to generate part of the map, and it must be taken into consideration whether the completed area is well fit to the original map. The local discriminator plays a role of a common discriminator in traditional GANs to judge whether the completed region is real or fake. And the global discriminator is a vital section to ensure the continuity of the whole map. What's more, the design of double discriminators can further increase the stability of the network during training.

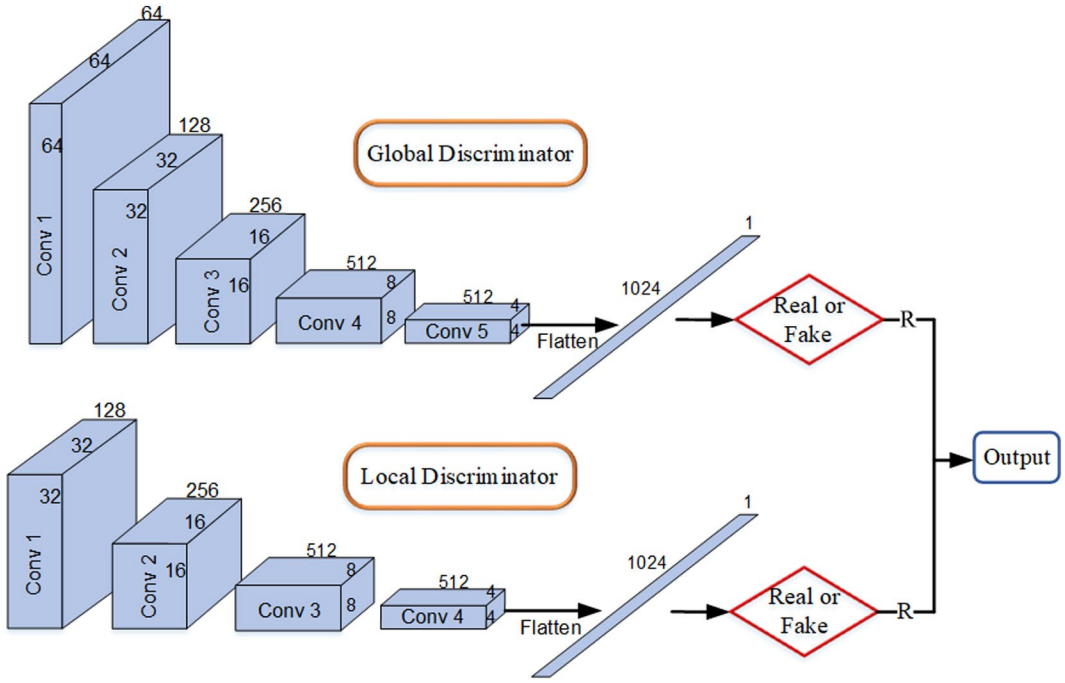

Figure 2. The structures of global discriminator and local discriminator. The final layers of both discriminators are the flatten layers which transfer the picture into a vector. According to the vector, the discriminators can judge the completed image whether real or fake and then output the image which is judged to be real as the result of GLGAN. GLGAN, Global and Local GAN.

3. Experiment

3.1. Data

The training data for the network are downloaded from Coordinated Data Analysis Web (https://cdaweb.gsfc.nasa.gov/index.html/). We choose GPS products which deduce 2-h TEC maps and movies. IGS Final-TEC Global Map is one of the products delivered by the IGS. The final IGS TEC maps are the average of products from four methods including CODE (University Bern, Switzerland), ESA (ESOC Darmstadt Germany), JPL (Jet Propulsion Lab, Pasadena USA) and UPC (University Politecnica Catalonia, Barcelona, Spain). The website provides the IGS TEC Global maps with CDF files since June, 1998. With the widespread GPS ground receivers and combination of different computation products, IGS TEC map receive high quality and credibility. Although the data of the area over the sea is still hard to obtain, the IGS TEC global map is the best choice for us to train to extract features of TEC maps and then fulfill the incomplete maps. The data from January 1, 2010 to June 30, 2012 with 10932 2-h IGS TEC global maps is selected to be the training data in the GL-GAN. And the testing set consists of 2171 IGS TEC maps from January 1, 2013 to June 30, 2013. We chose the data from 2010 to 2013, because the Sunspot tends to be more active during this period. And this period covers relatively quiet and high years of solar activity which is the common states of the space weather. Thus, the ability of generalization of the model may be enhanced, and the model may perform better in normal case. The original size of the data is 656×875 pixel. Before training, the size of the input data will be rescaled to 64×64 pixel.

It is vital to note that the training data set (2010–2012) is separate from the test data set (2013). The independence of the two data set is an insurance to prevent cheating the discriminator with an apparently good result of the completion network. If the test set consists of the components of the training set, the result will be better but doubtful and will lead to the ineffectiveness of the trained model.

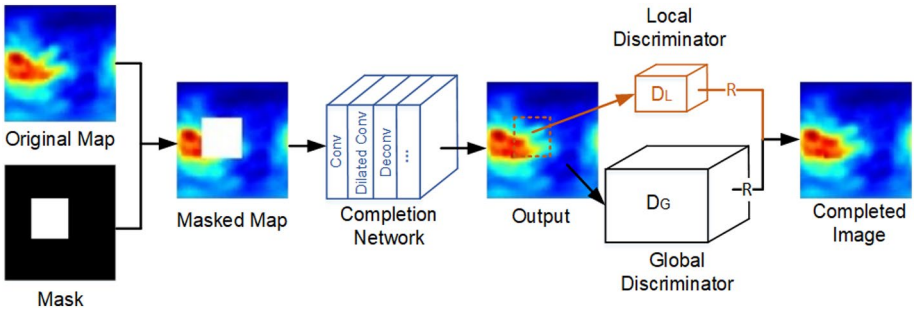

Figure 3. The structure of the global and local generative adversarial network (GLGAN). The mask consists of pixels filled with 0 and 1. The output of the completion network is the input of the local discriminator and global discriminator. If both discriminators think the output is true, then the final output of the GLGAN is the completed image.

3.2. Training

The input of the completion network for each iteration are an original map and a mask. The mask is a binary image with value of 0 and 1, which is used to generate the hole on the original image with random size and location. After linear combination of the two input images, the training image with a hole is obtained which will be feed to the completion network. Experiencing the whole completion network, the missing area of the training map has been completed. And the two discriminators are employed to judge the quality of the completed image. The basic process is clearly displaced in Figure 3. During the whole process, the optimization is a vital component of the network to drive the gradient decent which will bring about better results each iteration. When the gradient is nearly equals to 0, the iteration will be stopped and the completion network is often considered as the optimized model. The fundamental theory of the optimization is introduced as follows.

We define a functional operator $C\left(x,M_c\right)$ to denote the completion network, in which x denote the input map and M_c denote the mask of the input map. The size of the mask M_c is the same as the input map, and the value of the missing region is filled with 1 and other area is filled with 0. For each ground truth map x and mask M_c, our completion encoder network generates a output $C\left(x,M_c\right)$. In order to increase the reliability of training, two loss functions are combined to make up of the optimization (Pathak et al., 2016). The Mean Squared Error loss with a normalized L_2 distance is adopted as our reconstruction loss function $\mathcal{L}_{\text{rec}}$ which allows the training stability.

$$\mathrm{L}_{\text{rec}} = \| M_c \bullet \left(C\left(x,M_c\right) - x\right) \|^2, \tag{1}$$

where $\bullet$ is the element-wise multiplication operation and $\|\|$ is the Euclidean norm. The L_1 and L_2 losses have been found no significant difference. As a matter of fact, the L_2 loss often produces a blurry result and it tends to predict a mean value of the probability distribution. Thus, the adversarial loss is added to the loss function to help generate the distinct edges and corners.

The adversarial loss is also known as the GAN loss (Goodfellow et al., 2014). Together with the generative model (completion model in our paper), GAN simultaneously learns a discriminator model to generate the loss gradients for the generator. Then, the traditional optimization is turned into a min-max optimization problem, so that, the discriminator will update with the completion network each iteration.

$$\mathrm{L}_{\text{adv}} = \min_C \max_D \mathrm{E}\left[\log D\left(x,M_d\right)\log\left(1 - D\left(C\left(x,M_c\right),M_c\right)\right)\right]. \tag{2}$$

The functional operator $D\left(x,M_d\right)$ is defined to denote the combined discriminators, which contains both the global discriminator loss and the local discriminator loss. Both of the D and C are optimized by Stochastic Gradient Descent. And the joint loss $\mathcal{L}$ of the whole network is defined as

$$L = \lambda_{rec} L_{rec} + \lambda_{adv} L_{adv}, \tag{3}$$

where λ_{rec} and λ_{adv} are the weighing hyper parameters. In our study, the value of λ_{rec} and λ_{adv} is both set to be 1. That means the reconstruction loss and the adversarial loss have the same contribution to the joint loss. Note that the reconstruction loss prefers to represent the mean value of the completion area, while the adversarial loss tends to describe the subtle structures of the map. If the structure is blurry or we want to improve the global completion performance, we may appropriately change the percentage of the two loss functions which contributes to the overall loss function. To further combine the two loss function, the final overall loss function is defined as

$$L = \min_C \max_D E\left[\mathcal{L}_{rec} + \log D\left(x, M_d\right) + \alpha \log\left(1 - D\left(C\left(x, M_c\right), M_c\right)\right)\right], \tag{4}$$

where α is a weighing hyper parameter. In our study, α is set to be 1 to give more weight to the discriminator loss.

As is clearly shown in Figure 3, the input of the completion network is the training set of original IGS TEC maps and the random masks. The batch size of the training set is set as 64. What's more, the input size of the original map is rescaled as 64×64 pixel and the size of the patch is set to be 32×32 pixel (always larger than the size of the mask) rather than the size of the mask. Instead of generating the image from noise, we fill the masked area with constant mean value, which maintains the stability of the training process. Then, the completion network is trained to try to generate the miss area, while the discriminators are trained to distinguish the fake from the real. After nearly all of the convolutional layers, we add the batch normalization layers in both the completion network and the discriminator. In fact, each layer of both the completion network and the discriminator network is followed by a ReLU activation function (Hinton et al., 2010).

4. Results

We train the GL-GAN for total 400 epochs, and the loss tends to be steady with nearly no change. The training is performed with a single NVIDIA GeForce RTX 2080 graphics processing unit.

4.1. Completion Results of GL-GAN

Figure 4 shows the completion loss and global loss of GL-GAN decrease with the number of epoch. The whole GLGAN model is trained on the NVIDIA RTX 2080 GPU for total 400 epochs. Each epoch contains 171 steps with a batch size of 64, thus we get a data set consisting of 68,400 loss values as a result. An epoch is defined as a complete training data set which is transferred into the model, and the whole training data set is trained for 400 times in our model.

Figure 5 displays the completion results of the training data set. These 64 pictures are selected randomly from 171 batches of epoch 1. We collect the pictures into a matrix of 8×8, and the images are positioned with coordinates. These images represent the capability of the first trained completion network. Observe these images carefully, and we find the blurry area of the completion patch. For example, in a black rectangle in the graph with coordinates (1, 6), the patch covers the part of the bimodal structure in the maximum TEC area. As a result, the completion network fails to restore the feature of the structure. However, in the red rectangle in the image with coordinates (2, 6), the patch covers the part of minimum TEC area, and the completed area integrates into the environment well. Another problem occurs when we pay attention to the yellow rectangle in the image with coordinates (4, 8). The patch is selected to cover the edge of the image, and the abnormal values spread from the completed edge of the result. The similar condition appears in the image with coordinates (8, 8), which indicates the worse performance of the edge completion of the model.

After 400 iterations, the loss of the model has been stable and the completion network is fixed to have a steady performance. In order to evaluate the performance of the completion network, we construct the result-testing data set consisting of 1080 IGS TEC maps from January 1, 2016 to March 30, 2016. What has to note is that the evaluation data set (in 2016) are independent from the training data set (from 2010 to 2012) and the testing data set (in 2013), which is an important measure to prevent the double dipping problem.

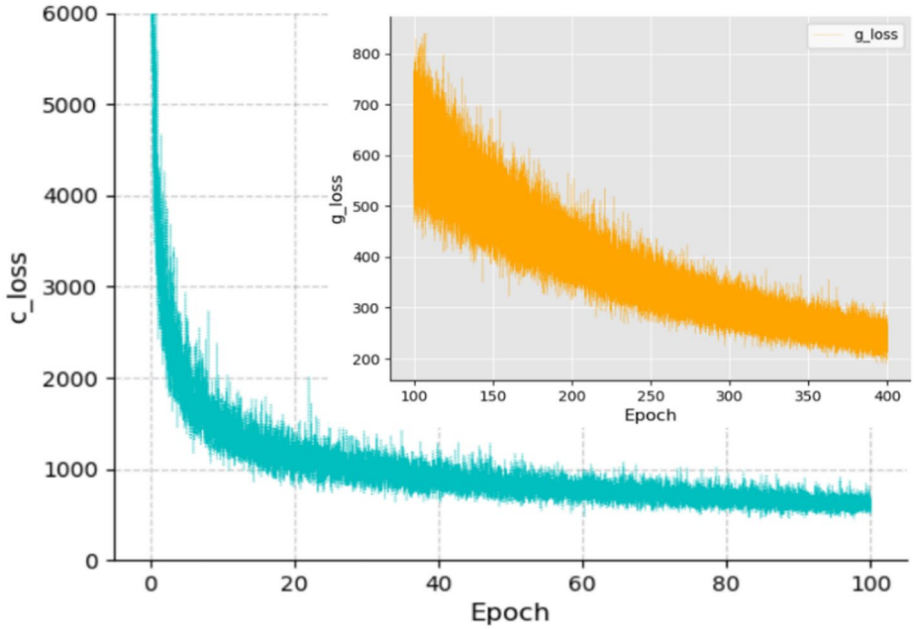

Figure 4. Completion loss and global loss both decrease with the number of epochs, and trend to be stable after 100 and 400 epochs. The line with cyan color represents the loss of completion network, and the line with orange color represents the global loss.

The double dipping problem is an illegal way to improve the results of the network in which part of the images from training data set or testing data set are inserted to the result-testing data set, which may lead to the better but unauthentic results. For example, if we put some same images into the training data set and the testing data set, the model will train the same images for two times. Because the model has trained the image, the model will obtain a better result when testing the image again. As a result, the model performs excellently on the testing data set, however, it is a disaster when the model is applied on other datasets. Make an assumption that the model can complete the image more similar to the repeatedly trained image better, and it will have worse performance on other images. That is to say, the model may be trapped in an overfitting problem and will be lack of the ability of generalization.

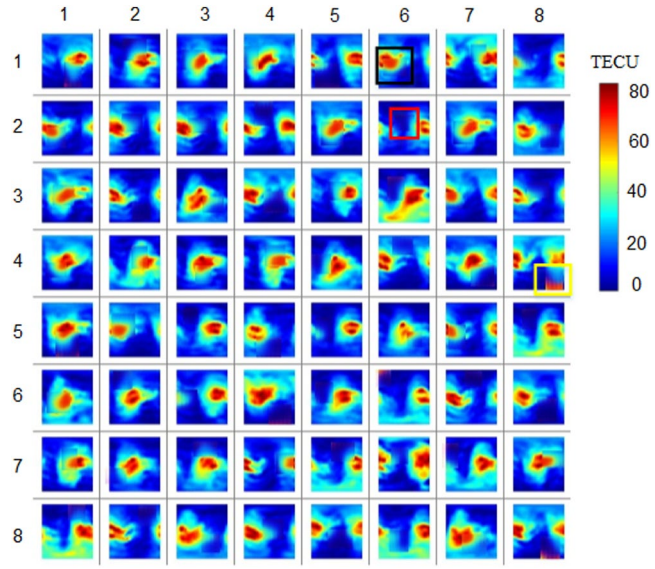

Figure 5. Completion results of the first epoch during training process. The batch size of the training data set is 64. The training data set consists of 10,932 images, about 171 batches, and this figure is results of the completion network during first training epoch selected from these batches. The rectangles with different colors are used to highlight the completion area of the images.

4.2. Quantitative Evaluation of Completion Network

To evaluate the completion results, we adopt a measure of structural similarity (SSIM) that compare the structural difference between two images (Zhou Wang et al., 2003). Instead of the luminance of the surface of an object, the SSIM evaluate the quality of the completed images from the structures of the object, which is separated from the illumination. Based on the study of Zhou Wang et al., we get a specific form of SSIM index as is shown in Equation 5

$$\mathrm{SSIM}(X,Y) = \frac{(2\mu_x\mu_y + C_1)(2\sigma_{xy} + C_2)}{(\mu_x^2 + \mu_y^2 + C_1)(\sigma_x^2 + \sigma_y^2 + C_2)}, \tag{5}$$

where $\mu_x, \mu_y, \sigma_x, \sigma_{xy}$ are the estimates of local statistics. Generally, C_1, C_2 are set to be zero, except the case that $(\mu_x^2 + \mu_y^2)$ or $(\sigma_x^2 + \sigma_y^2)$ is very close to zero. As a matter of fact, one only needs a single measure of the whole

image. When we use the SSIM index to evaluate the image, we prefer to adopt the mean SSIM index of the whole image.

$$\mathrm{MSSIM}(X,Y) = \frac{1}{M}\sum_{j=1}^{M}\mathrm{SSIM}(x_j, y_j). \tag{6}$$

In Figure 6, the test process and the SSIM distribution are clearly illustrated. The SSIM value of each pixel is ranging from 0 to 1. With the increase of the value, the difference between two pixels is smaller. That is to say, if the value is close to 1, the completed image is more similar to the original image, and the performance of the completion network is better. The mean SSIM value of Figure 6d is 0.9759. The image is selected from the evaluation data set. In order to evaluate the performance of the trained completion network, we construct an evaluation data set, which consists of 1,080 images from January 1, 2016 to March 30, 2016.

To further investigate the performance of the trained model in the common situation, we calculate the SSIM values of the 1,080 images in the evaluation data set. Considering that the SSIM of the whole image cannot reflect the results of the model exactly. We extract the missing part to calculate the SSIM between the missing part (Figure 7) and the completed missing part (Figure 7).

After calculating, the mean value of the SSIM of all of these images is 0.7467. As is shown in Figure 7, the values exist mostly around 0.8, which is higher than the mean value. And the median SSIM value in 2016 data set is 0.7886.

4.3. Results of Arbitrary Regions

Considering the size and location of each patch is set randomly during training, the fixed completion model is able to complete any patch of the image. To further investigate the ability of the model to complete arbitrary regions, we design a test program to make the random mask manually and complete the masked images with the fixed completion network.

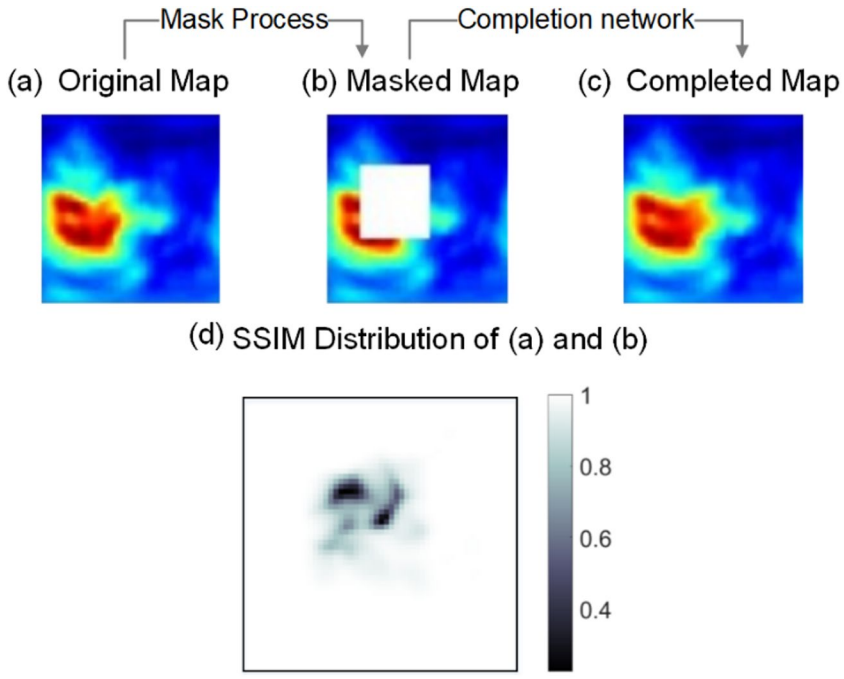

Figure 6. SSIM quality of the completed map and the original map. The process from (a) to (c) represent the process of completion. (a) is the original map selected from the result-testing data set (in 2016) and (b) is masked randomly from the (a). What's more, (c) is the completion result of (b). Figure (d) displays the distribution of the SSIM value between (a) and (b), and the SSIM value of the map is 0.9759. SSIM, structural similarity.

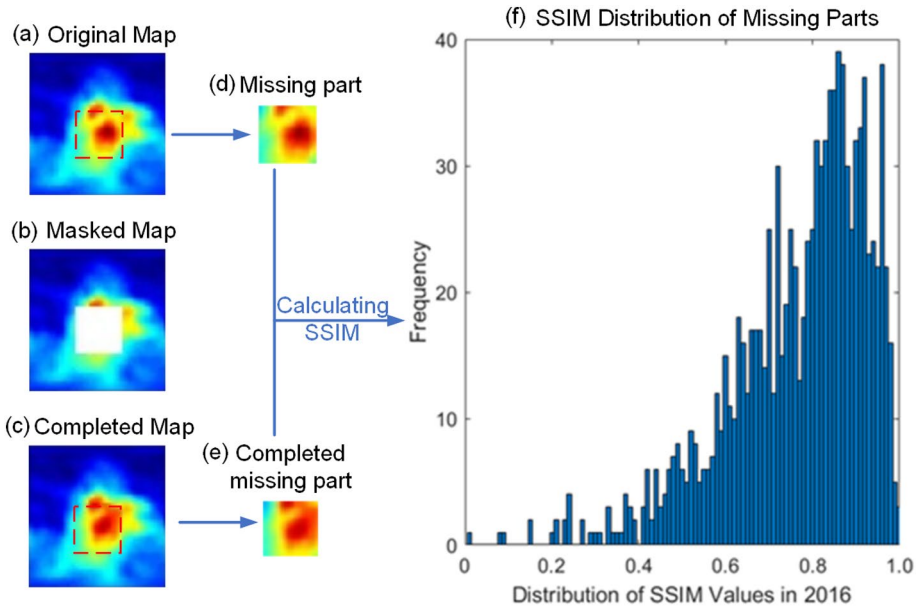

Figure 7. Calculating SSIM values of 1,080 images within the evaluation data set. (a) is the original map, and (d) is the masked area of (a). (c) is the completed map, and (e) is cut from (c) with the same coordinates and size as (d). (f) is the distribution of SSIM values of the data set between missing part and completed missing part just like (d) and (e). SSIM, structural similarity.

After examining the *Kp* index of all time during the evaluation data set, we choose several periods in January 1, 2016. According to the Kp index, there is a geomagnetic storm during 06:00–12:00 UT. The geomagnetic field trends to be quiet in other time. In order to test the performance of the completion network in arbitrary regions, the patch is masked manually. Focusing on the results of 00:00 UT in Figure 8, there are several little patches on different regions. One of these patches cover the TEC maxima region with complicated structure is completed better comparing with the TEC minimum region. It indicates a good performance of our model on completing the regions with complicated structures, where researchers may pay more attention on.

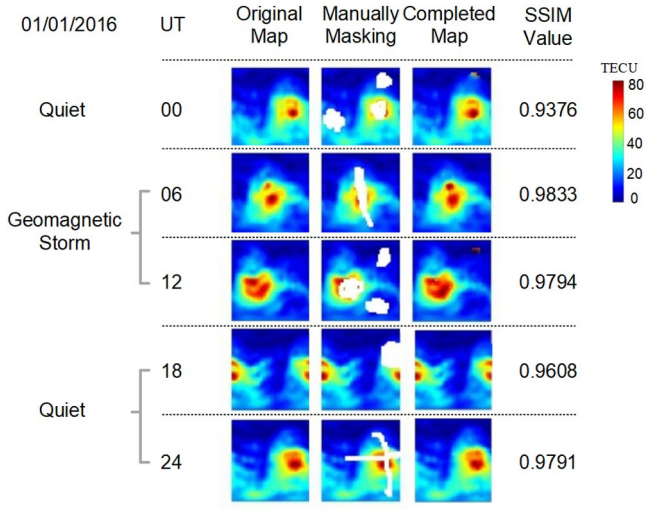

Figure 8. Completing arbitrary regions during geomagnetic storm time and quiet time. According to the geomagnetic data, the *Kp* index of UT 06 is 5.3, and UT 12 is 3.3, which indicates a geomagnetic storm during this period. The SSIM is calculated from the global images, due to the manually masked part is hard to extract and the SSIM is only used to make the comparison. SSIM, structural similarity.

What's more, comparing the results during geomagnetic storm time and quiet time 00:00 UT and 12:00 UT, 06:00 UT and 24:00 UT, the SSIM values of storm time are generally larger than that of quiet time. The storm time is recognized by the *Kp* index and don't take the phase of storm and electrodynamics of region into consideration. That is to say our GL-GAN model performs even better during storm time than quiet time. Considering the model performs well in complicated structures, one of the reasons for the better performance in storm time is that the geomagnetic storm triggers more complicated structures in TEC maximum regions. Additionally, the model has fixed the problem of performing badly in the edge of the image. Contract to the result boxed by the yellow rectangle in Figure 5, the result of UT 18 in Figure 8 demonstrates a good performance of the model in the edge. And the problem of color deviation disappears in the final model after the whole training process. What has to note is that, the images selected from the evaluation data set are totally separated from the training data set. Thus, our results of the final completion model achieve high reliability.

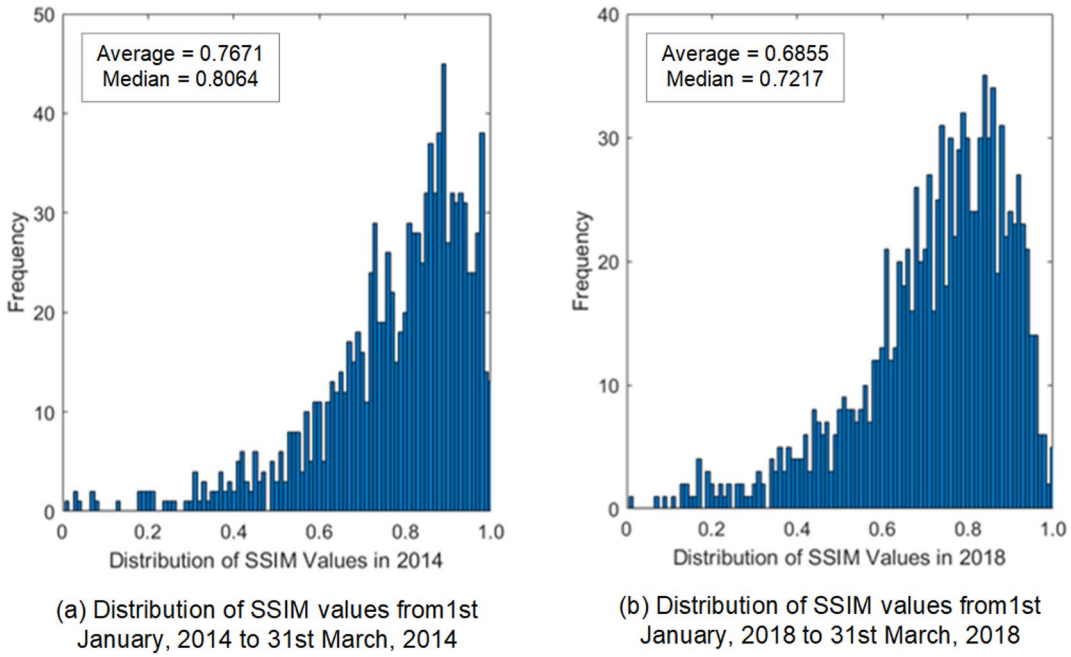

Figure 9. The distribution of SSIM values in 2014 (high solar activity year) and 2018 (low solar activity year). (a) shows the SSIM values in 2014, and the average is 0.7671, the median is 0.8064. (b) shows the SSIM values in 2018, and the average is 0.6855, the median is 0.7217. SSIM, structural similarity.

4.4. Comparison of Results During Years of High Solar Activity and Low Solar Activity

To further study the performance of our model during solar high years and low years, we selected the data set in 2014 (high solar activity year) and 2018 (low solar activity year). In order to avoid the impact of seasonal disturbance, we select the TEC maps from January 1, 2014 to March 31, 2014 and from January 1, 2018 to March 31, 2018. And we also calculate the SSIM of missing part and completed missing part to compare the results more exactly.

Figure 9 demonstrates the distribution of SSIM values during high solar activity year (2014, Figure 9a) and low solar activity year (2018, Figure 9b). It is clear that the most value appear in the interval (0.8–0.9) in 2014, and (0.7–0.8) in 2018. What's more, the mean value in 2014 is 0.7671, larger than that in 2018 which is 0.6855. In order to prevent individual minimum values from having a greater impact on the average, we also calculate the median of all of the values. The median can also reflect the data distribution intervals. And the median in 2014 is 0.8064, the median in 2018 is 0.7217. This results suggests that the common distribution of SSIM values in 2018 is lower than that in 2014. That is to say, our model performs better in the high solar activity years. We propose several possible reasons to try to explain this result. In terms of the formation mechanism of the TEC map, in high solar activity years, the solar activity may have more effect on the complicated structures on the TEC maps than many other uncertain and small-scales disturbance. However, in low solar activity years, these uncertain disturbance is a main factor in the formation of the complicated structures on the TEC maps. Thus, it is harder for the model to reconstruct the disturbance on the TEC maps in low solar activity years. In terms of the ability of the model, the model is good at extracting the features of the images. In high solar activity years, the feature of some vital regions such as “Equatorial double hump region” seems to be more obvious and more complicated. It is easier for the GLGAN model to learn the obvious features on the TEC maps, and may obtain the better completion result. With further research, many advantages and characters of GLGAN will be better explained.

5. Conclusions

In this paper, we propose a new deep learning method GLGAN to complete the global TEC map. With the development of Generative Adversarial Network theory, more and more reformation of GANs perform well in the translation from image to image. The traditional GAN often generates a totally new image from a probability distribution. However, the global TEC map is always lack of little data in some key areas. The direct application of the traditional GAN may increase the instability of the new image. In order to complete the image only in the missing region and keep the stability of the whole image, we apply a new method GLGAN which can complete any shape of regions and discriminate the result locally and globally. The whole GLGAN consists of a generative network which is known as the completion network and two discriminating networks (including a local discriminator and a global discriminator). The training data set is selected from the IGS global TEC maps per 2 h. The IGS TEC map is widely considered as the true data of the time varying ionosphere. With the assistant of the GLGAN, we can obtain the special characteristic of the TEC distribution and different structures in different time, and then generate the quasi real TEC map even with the absence of some vital data in key areas quickly.

During the design and construction of the network, we adopt some tricks to improve the performance of GLGAN. In the completion network, the dilated convolution layers are applied to enlarge the visual field around the pixels with the same parameters and calculation ability. This improvement can help the completion network to obtain more information around the missing areas and make the completed data be consistent to the whole map. As a matter of fact, the dilated convolution layer can increase the accuracy and efficiency of the completion network greatly. Within the completion network, the resolution of imaged is only decreased two times, which avoids the blurring regions of the completion network. The input and the output of the completion network are set to be $64 \times 64 \times 3$, which keeps the same quality and size as the original map. In the discriminator, we develop two networks named as global discriminator and local discriminator to enhance the ability to figure out whether the output of the completion network is real or fake. The size of the input in local discriminator is set to be $32 \times 32 \times 3$, which is the half size of that in global discriminator. The design of two discriminators enhances the ability of discriminator a lot, and thus improves the performance of the completion network indirectly. We test different learning rate during training, and finally set it to be 0.001 to accelerate the rate of loss decline. The parameter α in Equation 4 is set to be 1 to give more weight to the discriminator loss. However, the better set of the hyperparameters deserves further investigation.

What's more, we adopt the SSIM method to evaluate the quality of the completed images. After comparing the results during storm time and quiet time, the GLGAN has better performance in completing the map in storm time. And it can also complete the edge of the image well. It is vital to emphasize that the training data set, the test data set and the evaluation data set are totally separated with each other. Which means the images used in these datasets are not reused or mixed. Thus, the results developed from the quantitative evaluation is reliable.

This paper demonstrates a new possibility for the application of deep learning on the geoscience. Not only the global TEC maps, but also many other parameter maps (such as the f_0F_2, the electron density and the density of neutral particles) face the same problem of missing data in some areas. Our GLGAN model can be improved properly to solve the similar problems. However, further research is also necessary to make the GLGAN method more reliable. The theory of the GAN comes into a bottleneck, which may impede the development of the deep learning in the geoscience. Furthermore, the GLGAN itself has some drawbacks. Up to now, the completion network still cannot complete the image with very large scale of missing data areas, although the dilated convolution layers have enhanced related ability a lot. Besides, the experiment of testing the model in the data set with higher resolution also calls for more efficient training equipment and improved network structures. Except the global TEC maps, researchers may pay more attention to local TEC maps. Considering the better performance of GLGAN on the complicated structures, the application on the local TEC maps with higher resolution may achieve more significant results.

Data Availability Statement

The TEC datasets are downloaded from the Coordinated Data Analysis Web Coordinated Data Analysis Web (https://cdaweb.gsfc.nasa.gov/index.html/). The main programs (Python/TensorFlow) of our work in this paper is available on figshare (https://www.doi.org/10.6084/m9.figshare.13480377).

Acknowledgments
This research was supported by the National Natural Science Foundation of China (No. 41804149).

References

Chen, Z., Jin, M., Deng, Y., Wang, J. S., Huang, H., Deng, X., et al. (2019). Improvement of a deep learning algorithm for total electron content (TEC) maps: Image completion. *Journal of Geophysical Research: Space Physics*, *124*(1), 790–800. https://doi.org/10.1029/2018JA026167

Chua, L. O., & Roska, T. (1993). The CNN paradigm. *IEEE Transactions on Circuits and Systems I: Fundamental Theory and, Applications*, *40*(3), 147–156. https://doi.org/10.1109/81.222795

Coster, A., & Komjathy, A. (2008). Space weather and the global positioning system. *Space Weather*, *6*, S06D04. https://doi.org/10.1029/2008SW000400

Deng, Y., Dai, Q., & Zhang, Z. (2011). Graph Laplace for occluded face completion and recognition. *IEEE Transactions on Image Processing*, *20*(8), 2329–2338. https://doi.org/10.1109/TIP.2011.2109729

Feltens, J. (2003). The international GPS service (IGS) ionosphere working group. *Advances in Space Research*, *31*(3), 635–644. https://doi.org/10.1016/S0273-1177(03)00029-2

Fukushima, K. (1988). Neocognitron: A hierarchical neural network capable of visual pattern recognition. *Neural Networks*, *1*(2), 119–130. https://doi.org/10.1016/0893-6080(88)90014-7

Goodfellow, I., Pouget-Abadie, J., Mirza, M., Xu, B., Warde-Farley, D., Ozair, S., et al. (2014). Generative adversarialnets. In Z. Ghahramani, M. Welling, C. Cortes, N. D. Lawrence, & K. Q. Weinberger, Eds., *Advances in neural information processing systems* (Vol. *27*, pp. 2672–2680). Canada:Curran Associates, Inc. Retrieved from https://papers.nips.cc/paper/5423-generative-adversarial-nets.pdf

Hernández-Pajares, M., Juan, J. M., Sanz, J., Orus, R., Garcia-Rigo, A., Feltens, J., et al. (2009). The igs vtec maps: A reliable source of ionospheric information since 1998. *Journal of Geodesy*, *83*(3–4), 263–275. https://doi.org/10.1007/s00190-008-0266-1

Iizuka, S., Simo-Serra, E., & Ishikawa, H. (2017). Globally and locally consistent image completion. *ACM Transactions on Graphics*, *36*(4), 1–14. https://doi.org/10.1145/3072959.3073659

Jakowski, N., Heise, S., Wehrenpfennig, A., Schlüter, S., & Reimer, R. (2002). Gps/glonass-based TEC measurements as a contributor for space weather forecast. *Journal of Atmospheric and Solar-Terrestrial Physics*, *64*(5–6), 729–735. https://doi.org/10.1016/s1364-6826(02)00034-2

Ji, E. -Y., Moon, Y. -J., & Park, E. (2020). Improvement of IRI global TEC maps by deep learning based on conditional generative adversarial networks. *Space Weather*, *18*(5). https://doi.org/10.1029/2019SW002411

Krizhevsky, A., Sutskever, I., & Hinton, G. (2012). ImageNet Classification with Deep Convolutional Neural Networks. *NIPS'12: Proceedings of the 25th International Conference on Neural Information Processing Systems* (Vol. 1, pp. 1097–1105). Retrieved from https://doi.org/10.1145/3065386

Ledig, C., Theis, L., Huszar, F., Caballero, J., Cunningham, A., Acosta, A., et al. (2016). Photo-realistic single image super-resolution using a generative adversarial network. *Paper presented at 2017 IEEE Conference on computer Vision and pattern recognition (CVPR)*. IEEE. Retrieved from https://doi.org/10.1109/CVPR.2017.19

Leinonen, J., Guillaume, A., & Yuan, T. (2019). Reconstruction of cloud vertical structure with a generative adversarial network. *Geophysical Research Letters*, *46*, 7035–7044. https://doi.org/10.1029/2019GL082532

Mannucci, A. J., Wilson, B. D., Yuan, D. N., Ho, C. H., Lindqwister, U. J., & Runge, T. F. (1998). A global mapping technique for GPS-derived ionospheric total electron content measurements. *Radio Science*, *33*(3), 565–582. https://doi.org/10.1029/97rs02707

Nair, V., & Hinton, G. E. (2010). Rectified linear units improve restricted boltzmann machines. *ICML'10: Proceedings of the 27th International Conference on International Conference on Machine Learning* (pp. 807–814). Retrieved from https://dl.acm.org/doi/10.5555/3104322.3104426

Orús, R., Hernández-Pajares, M., Juan, J. M., & Sanz, J. (2005). Improvement of global ionospheric VTEC maps by using kriging interpolation technique. *Journal of Atmospheric and Solar-Terrestrial Physics*, *67*(16), 1598–1609. https://doi.org/10.1016/j.jastp.2005.07.017

Pathak, D., Krahenbuhl, P., Donahue, J., Darrell, T., & Efros, A. A. (2016). Context Encoders: Feature Learning by Inpainting. *2016 IEEE Conference on Computer Vision and Pattern Recognition (CVPR)* (pp. 2536–2544). Retrieved from https://ieeexplore.ieee.org/document/7780647

Radford, A., Metz, L., & Chintala, S. (2015). Unsupervised Representation Learning with Deep Convolutional Generative Adversarial Networks. *arXiv e-prints*. Retrieved from https://arxiv.org/abs/1511.06434

Rao, S. S., Chakraborty, M., Pandey, R., & Singh, A. K. (2019). Fof 2 variability at the southern low latitude station and the performance of iri-2016 model during ascending phase of solar cycle-24. *Advances in Space Research*, *64*(11), 2269–2279. https://doi.org/10.1016/j.asr.2019.08.014

Salimans, T., Goodfellow, I., Zaremba, W., Cheung, V., Radford, A., & Chen, X. (2016). Improved Techniques for Training GANs. *NIPS'16: Proceedings of the 30th International Conference on Neural Information Processing Systems* (pp. 2234–2242). Retrieved from https://dl.acm.org/doi/abs/10.5555/3157096.3157346

Yu, F., & Koltun, V. (2015). Multi-Scale Context Aggregation by Dilated Convolutions. *ICLR 2016*. Retrieved from https://arxiv.org/abs/1511.07122

Zhou, W., Alan Conrad, B., & Hamid, R. S. (2003). Image quality assessment: From error visibility to structural similarity. *IEEE Transactions on Image Processing*, *13*(4), 600–612. https://doi.org/10.1109/TIP.2003.819861